D. C. Joy, Ed., *Analytical Electron Microscopy — 1987*
Copyright © 1987 by San Francisco Press, Inc., Box 6800, San Francisco, CA 94101-6800, USA

AEM DETERMINATION OF COMPOSITION PROFILES FORMED DURING CELLULAR PRECIPITATION IN Ni-In ALLOYS

K. B. Alexander and D. E. Laughlin

Cellular precipitation occurs in a wide range of alloys and is generally associated with a degradation in mechanical and electrical properties. In order to suppress the reaction, the factors that govern the kinetics of the reaction must be understood. Many theories have been proposed to account for the growth kinetics of cellular precipitation. To compare the observed growth kinetics with any theoretical model, several parameters must be measured: the growth velocity, the interlamellar spacings involved, and the amount of nonequilibrium segregation retained in the α lamellae. This last parameter has often been measured by x-ray diffraction methods. However, microanalytical techniques in the transmission electron microscope have proved to be much more informative.

Experimental Procedure

Energy-dispersive x-ray spectroscopy was performed in the STEM mode in a Philips 420T, with a 20° elevated detector and the sample tilted 10° toward the detector. The cellular reaction front was oriented as shown in Fig. 1 to optimize the microanalysis from the interlamellar regions. Ni-Kα and In-Lα lines were used for the quantitative analysis. The foil thickness at the microanalysis location was determined by convergent beam electron diffraction and confirmed by the use of the thickness determined from the distance between contamination deposits on samples tilted 45°. The spot size and condenser apertures used were chosen to minimize the "halo" of spherically aberrated electrons outside the intense central beam. Probe sizes used were 10 to 30 nm. Attempts were made to acquire at least 3000 counts in the indium Lα peak. Several Ni-In alloys of known composition were used to obtain $k_{In\text{-}L\alpha/Ni\text{-}K\alpha}$ to convert X_{In}/X_{Ni} (intensities) to C_{In}/C_{Ni} (compositions). The experimental compositions were corrected for absorption effects. The results of the absorption corrections as a function of thickness in a well-annealed sample are shown in Fig. 2. The interlamellar spacings were measured from TEM micrographs with the lamellae oriented in an edge-on configuration, whereas the growth velocities were measured for the colony of interest directly from the thinned TEM foil in a scanning electron microscope.

Author Alexander, formerly of Carnegie-Mellon University, is now at Metals and Ceramics Division, Oak Ridge National Laboratory, Oak Ridge, TN 37831-6376. Author Laughlin is at Carnegie-Mellon University, Department of Metallurgical Engineering and Materials Science, Pittsburgh, PA 15227. This research was supported by NSF grant DMR-8413115, the Amelia Earhart Zonta International Fellowship (KBA), and the Division of Materials Science, U.S. Dept. of Energy under contract DE-AC05-84OR21400 with Martin Marietta Energy Systems, Inc.

Cellular Precipitation in Ni-In Alloys

During cellular precipitation, a two-phase lamellar product is formed behind a migrating boundary. This reaction can be expressed as $\alpha_0 = \alpha + \beta$, where α_0 is the original supersaturated matrix and α and β are the components of the two-phase lamellar product. As a result of cellular precipitation, nonequilibrium segregation necessarily occurs within the α lamella. The determination of the degree of segregation in this region is necessary to quantify the growth kinetics of cellular precipitation. Following Cahn[1] and Sundquist,[2] the solution to the diffusion equation governing the redistribution of solute in the α lamella can be written as:

$$\frac{x_0 - x_\alpha}{x_0 - x_3} = \frac{\cosh[\sqrt{a}(z/S_\alpha)]}{\cosh(\sqrt{a}/2)} \qquad (1)$$

$$\text{where } a = \frac{v\, S_\alpha^2}{\cos\theta|_{avg}\, kD_b\delta} \qquad (2)$$

and x_0 is the alloy composition; x_α is the position-dependent composition within the α lamella; x_3 is the composition at the α/β interface, which, due to capillarity is not necessarily equal to $x_e^{\alpha\beta}$, the equilibrium α composition; z is a distance across the α lamella; v is the growth velocity; S_α is the interlamellar spacing of the α lamella; k is the grain boundary segregation coefficient; D_b is the grain boundary diffusion coefficient; δ is the grain boundary thickness; and θ is the angle between the global growth direction and the local reaction front normal. The dimensionless parameter a reflects the amount of nonequilibrium segregation retained in the α lamellae. For large values of a the solute profile in the α lamella is very steep, whereas for small a , the solute profile is very flat. For experimentally determined α phase interlamellar solute profiles, the two unknown values (a and x_3) can be determined by nonlinear regression analysis from Eq. (1).

precipitation for two reasons: (1) there is very little prior matrix precipitation, which is a necessary condition to treat the untransformed matrix thermodynamically as a solid solution of α of composition x_0; and (2) the system is suitable for use of energy-dispersive x-ray spectroscopy (EDS) to determine the solute profiles within the α lamella. The alloy compositions, aging temperatures, and aging times were chosen so that the interlamellar

spacings were larger than 0.2 μm and that substantial growth (>10 μm) occurred in a few minutes. Solute depletion was often observed prior to the appearance of the cellular lamellar structure. Figure 3 shows a solute-depleted region between the original grain boundary location and the initiation of the lamellar structure. This depletion has also been observed in Al-Zn alloys, and it has been proposed that diffusion-induced grain boundary migration (DIGM) processes are responible.[3] A solute profile obtained in a Ni 4.6 at.% In alloy is shown in Fig. 4. The a and x_3 values calculated by nonlinear regression analyses from Eq. (1) are also shown. Figure 5 shows a STEM micrograph along with the solute profile obtained across the α lamella.

Discussion

The growth kinetics can be modeled, following Hillert,[4-6] by balancing the forces on the α and β lamellae individually. The forces acting on each portion of the reaction front include: a chemical driving force (+), a surface energy term to create new σ_{ab} interfaces (-), and a drag force term since the boundary is not infinitely mobile (-). By assuming a parabolic free-energy expression and solving these equations for both the α and β lamellae, a series of solutions relating the growth velocity and the interlamellar spacing S_a is obtained. In Fig. 6, the velocity-spacing relationship is plotted in dimensionless parameters for several values of the dimensionless mobility $m = MS_{rev}\sigma/kD_b\delta$, where $S_{rev} = 2\sigma V_m/\Delta G_{tot}$ is the spacing that would be observed if all the free energy available (ΔG_{tot}) were used to create new interfacial area and M is the grain boundary mobility. For Ni-In, σ was assumed[7] to be 0.56 J/m^2 and the molar volumes V_m used were those calculated by Graf.[8] The growth velocities and spacings measured in this study are also plotted in Fig. 6. In previous work[4,5] it was assumed that the drag force on the boundary was negligible ($m = \infty$). However, the present results indicate that the drag force term is significant with m values of the order of 0.10 to 0.50. From these dimensionless mobility values, the mobility M can be calculated and is consistent with those usually obtained in DIGM experiments ($M \cong 10^{-15}$ m^4/J s). More detailed comparisons of the growth kinetics model with the present data and with previous investigators' results can be found in Ref. 7.

By writing a force balance for each point along the lamella, where the surface energy term is now that due to the local radius of curvature, the shape of the reaction front can be calculated by solving for the radius of curvature at each point along the lamella.[7] Figure 7 shows the reaction front calculated from the solute profile and m value (0.25) appropriate for the cellular colony shown in Fig. 5. The observed reaction front shape agrees very well with that predicted from the growth kinetics model. Much larger values of m result in reaction front shapes that are very convex; i.e., the reaction front bows forward toward the untransformed matrix. Since the reaction front is nonplanar, the distances over which diffusion must occur are larger than $S_\alpha/2$. Solving the growth kinetics equations iteratively with the reaction front shape equations results in a maximum spacing (S_{max}) beyond which there are no steady-state solutions. At this maximum spacing, the reaction front develops a deep recess, which results in a very steep concentration profile due to the longer diffusion distances involved. At spacings above the maximum spacing, the diffusion distances become so large and the profiles so steep that it is impossible for all points along the reaction front to migrate forward with the same velocity. However, re-entrant reaction front shapes favorably orient portions of the boundary for nucleation of a new lamella, thus permitting steady-state growth to continue should the spacing diverge beyond the maximum steady-state spacing. There also exists a minimum spacing due to the shape of the velocity-spacing curve. The spacing S_{min} associated with the maximum velocity will outgrow spacings with $S_\alpha < S_{min}$. Therefore, only spacings with $S_{min} < S_\alpha < S_{max}$ should ever be observed. The maximum allowable spacing S_{max} for m = 0.1 is marked on Fig. 6. (S_{max} for m = 0.5 is just beyond $S_\alpha/S_{rev} = 12.0$.)

Conclusions

The solute profiles in the α lamellae during cellular precipitation in Ni-In alloys can be accurately measured by x-ray microanalysis. The advantage of this method over x-ray diffraction methods to determine a are

1. There are no spurious contributions to the composition measurements from solute depletion which occurs prior to cellular precipitation (Fig. 3).
2. Often, the spacings of adjacent lamellae vary quite dramatically. Using microanalysis, the exact relationship of velocity, spacing, and a can be determined for individual lamellae.

This model summarized in this paper is based on Hillert's treatment of the growth kinetics of cellular precipitation. With this model, it is clear that the drag force term is a significant factor in cellular precipitation. The calculated mobility values M are consistent with those observed during DIGM processes and the growth front shapes observed are similar to those predicted with small m values. The model predicts an upper bound on the observable spacing. The lower bound is the spacing possessing the maximum growth velocity. The experimental data obtained from Ni-In alloys all lie within the predicted range of permissible spacings.

References

1. J. W. Cahn, *Acta Met.* 3: 55, 1955.
2. B. E. Sundquist, *Met. Trans.* 4: 1919, 1973.
3. I. G. Solorzano, Ph.D. diss. MacMaster U., 1983.
4. M. Hillert, *The Mechanism of Phase Transformations in Crystalline Solids*, London: Institute of Metals, 1969, 231.
5. M. Hillert, *Acta Met.* 30: 1689, 1982.
6. M. Hillert, *Met. Trans.* 3: 2729, 1972.
7. K. B. Alexander and D. E. Laughlin, *Acta Met.* (submitted).
8. W. Graf, Ph.D. diss. U. Münster, 1983.

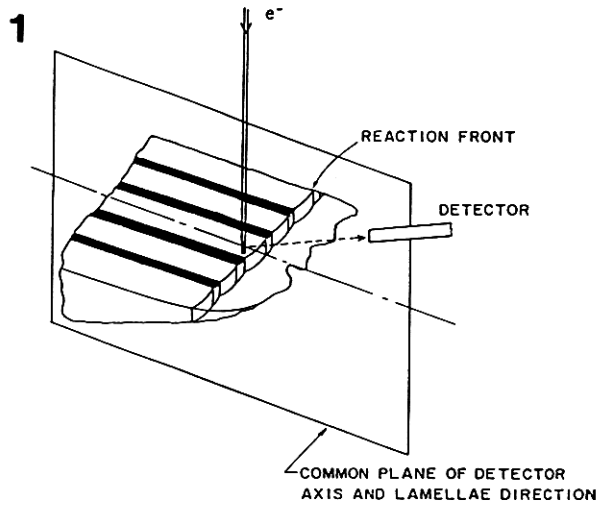

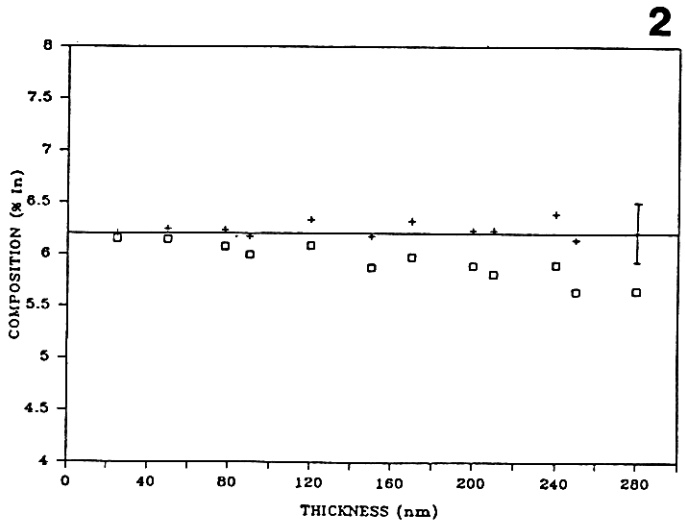

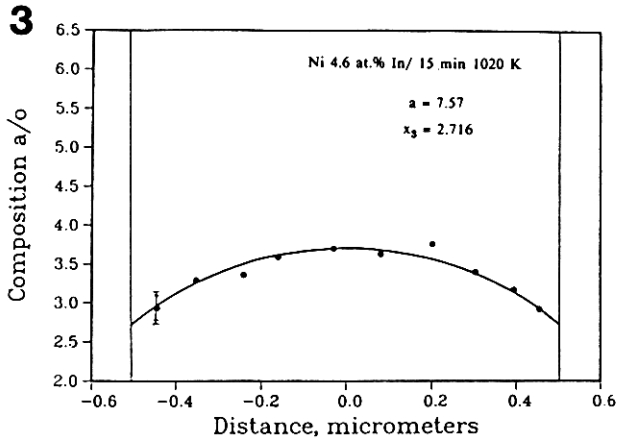

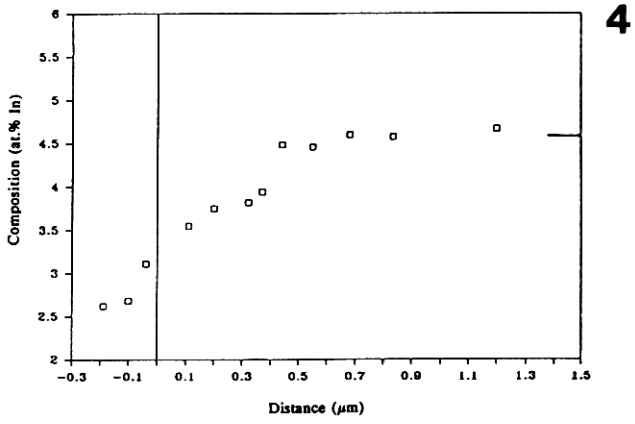

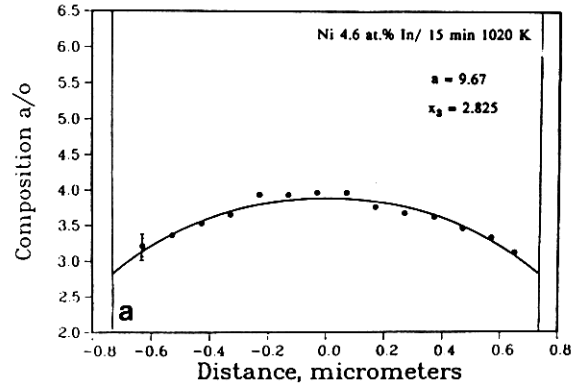

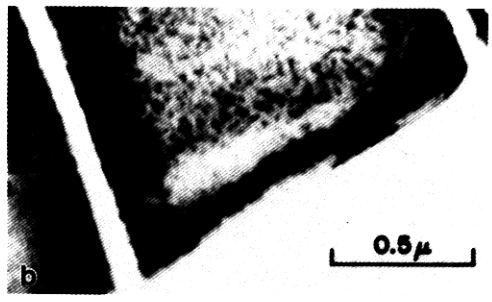

FIG. 1.--Schematic microanalysis geometry.
FIG. 2.--Effects of absorption correction as a function of foil thickness. Squares represent original uncorrected data; crosses, absorption corrected data.
FIG. 3.--Microanalysis across original grain boundary site. Cellular portion is on left, original grain boundary site on right. Growth direction is from right to left.
FIG. 4.--Composition profile for Ni-4.6 at.% In aged 15 min at 1020 K. Error bars represent 95% and 99% confidence intervals on data.
FIG. 5.--(a) Composition profile across α lamella shown in STEM micrograph (b). Slight contamination spots can be seen at microanalysis locations.

6

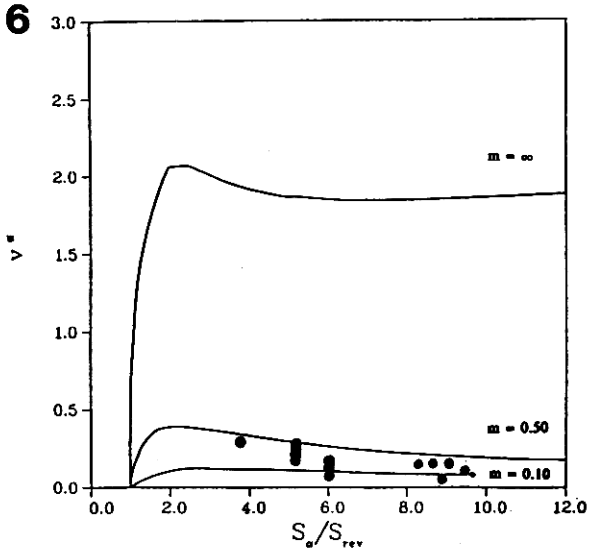

7

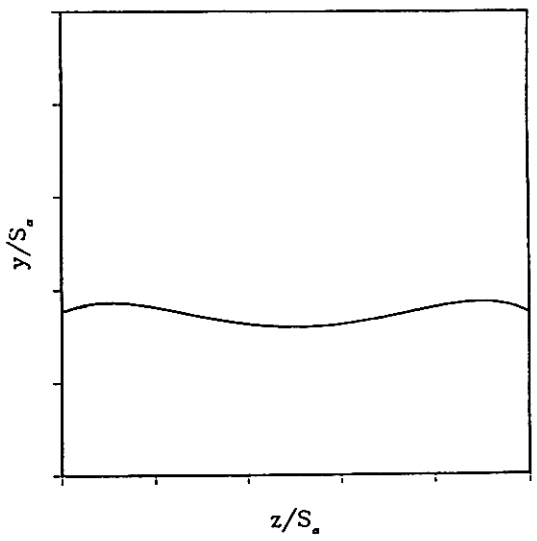

FIG. 6.--Dimensionless velocity $v^* = vS_{rev}^2/kD_b$ plotted against dimensionless spacing for various values of dimensionless mobility m.
FIG. 7.--Reaction front shape calculated with experimental parameters associated with reaction front shown in Fig. 5.